

Extracting the temperature dependence in high- p_{\perp} particle energy loss

Stefan Stojku ¹, Bojana Ilic ¹, Marko Djordjevic ² and Magdalena Djordjevic ^{1,*}

¹*Institute of Physics Belgrade, University of Belgrade, Belgrade, Serbia*

²*Faculty of Biology, University of Belgrade, Belgrade, Serbia*



(Received 16 July 2020; accepted 2 February 2021; published 16 February 2021)

The suppression of high- p_{\perp} particles is one of the main signatures of parton energy loss during its passing through the quark-gluon plasma medium, and is reasonably reproduced by different theoretical models. However, a decisive test of the reliability of a certain energy-loss mechanism, apart from its path length, is its temperature dependence. Despite its importance and comprehensive dedicated studies, this issue is still awaiting more stringent constraints. To this end, we here propose a novel observable to extract the temperature-dependence exponent of a high- p_{\perp} particle's energy loss, based on R_{AA} . More importantly, by combining analytical arguments, full-fledged numerical calculations, and comparison with experimental data, we argue that this observable is highly suited for testing the long-standing $\Delta E/E \propto L^2 T^3$ paradigm. The anticipated significant reduction of experimental errors will allow direct extraction of temperature dependence, by considering different centrality pairs in $A + A$ collisions (irrespective of the nucleus size) in the high- p_{\perp} region. Overall, our results imply that this observable, which reflects the underlying energy-loss mechanism, is very important to distinguish between different theoretical models.

DOI: [10.1103/PhysRevC.103.024908](https://doi.org/10.1103/PhysRevC.103.024908)

I. INTRODUCTION

The main goal of the ultrarelativistic heavy-ion program [1–4] at the Relativistic Heavy Ion Collider (RHIC) and the Large Hadron Collider (LHC) is inferring the features of the created novel form of matter—quark-gluon plasma (QGP) [5,6]—which provides an insight into the nature of the hottest and densest known medium. Energy loss of rare high- p_{\perp} partons traversing the medium is considered to be one of the crucial probes [7] of the medium properties, which also had a decisive role in QGP discovery [8]. Comparison of predictions stemming from different energy-loss models with experimental data tests our understanding of the mechanisms underlying the jet-medium interactions, thereby illuminating the QGP properties. Within this, an important goal involves a search for adequate observables for distinguishing the energy-loss mechanisms.

Connected to this, it is known that the temperature (T) dependence of the energy-loss predictions may be related to the underlying energy-loss mechanisms; e.g., pQCD *radiative* energy loss (Baier-Dokshitzer-Mueller-Peigne-Schiff (BDMPS) and Armesto-Salgado-Wiedemann (ASW) [9–11], Gyulassy-Levai-Vitev (GLV) [12], light-cone path integral (LCPI) [13] and Arnold-Moore-Yaffe (AMY) [14], higher-twist (HT) [15], and some of their extensions [16–20]) is typically considered to have cubic T dependence (T^3 , stemming from entropy, or energy density dependence), while *collisional* energy loss [7,21–23] is generally considered to be proportional to T^2 . Additionally, anti-de Sitter/conformal field

theory (AdS/CFT)-motivated jet-energy-loss models [24,25] display even quartic (T^4) dependence on temperature. The different functional dependences on T found in these models are the results of the considered energy-loss mechanism (elastic or inelastic), different treatment of the QCD medium (finite or infinite size), and inclusion or omission of finite temperature effects (i.e., application of temperature-modified or vacuumlike propagators). Therefore, assessing the accurate temperature dependence is important for disentangling relevant effects for adequate description of leading parton energy loss, and consequently for understanding the QGP properties.

For a comprehensive study on temperature (and path-length) dependence of different energy-loss models we refer the reader to Ref. [18]. However, even this systematic study could not single out local T dependence, as the attempt to simultaneously describe high- p_{\perp} R_{AA} and v_2 data within these models requires some more rigorous physical justifications. Moreover, the current error bars at the RHIC and the LHC are still too large to resolve between different energy-loss models. Having this in mind, we here propose a novel observable to extract the scaling of a high- p_{\perp} particle's energy loss on the local temperature. Note that, for extracting the exact value of the temperature-dependence exponent, this new observable relies on the previously extracted value of the path-length dependence coefficient [26]. We expect that this observable will allow direct extraction of T dependence from the data in the upcoming high-luminosity third run at the LHC, where the error bars are expected to notably decrease.

We also propose high- p_{\perp} h^{\pm} as the most suitable probe for this paper, as the experimental data for h^{\pm} R_{AA} are more abundant and with smaller error bars, compared to heavier hadrons for all centrality classes, where this is also expected

* magda@ipb.ac.rs

to hold in the future. Therefore, in this paper, we concentrate on h^\pm in 5.02-TeV Pb + Pb collisions at the LHC, with the goal to elucidate this new observable, and test its robustness to medium evolution and colliding system size. By combining full-fledged numerical predictions and scaling arguments within our dynamical radiative and elastic energy-loss approach (DREENA) [27,28] framework, this new observable yields the value of the temperature-dependence exponent, which is in accordance with our previous estimate [29]. More importantly, we utilize this observable to question the long-standing $\Delta E/E \propto L^2 T^3$ paradigm, used in a wide range of theoretical models [9–12,15–20].

II. THEORETICAL FRAMEWORK

In this paper, we use our state-of-the-art dynamical energy-loss formalism [30–32], which includes several unique features in modeling jet-medium interactions: (1) calculations within the finite temperature field theory and generalized hard-thermal-loop approach [33] (contrary to many models

which apply vacuumlike propagators [9,10,12,15]), so that infrared divergences are naturally regulated in a highly non-trivial manner; (2) finite size of created QGP; (3) the QCD medium consisting of dynamical (moving) as opposed to static scattering centers, which allows the longitudinal momentum exchange with the medium constituents; (4) both radiative [30,31] and collisional [32] contributions calculated within the same theoretical framework; (5) the inclusion of a finite parton's mass [34], making the formalism applicable to both light and heavy flavor; and (6) the generalization to a finite magnetic mass [35], running coupling [36], and beyond soft-gluon approximation [37]. Note, however, that in Ref. [37] we obtained that the effect of relaxing the soft-gluon approximation on (fractional radiative energy loss and) R_{AA} is negligible, and thus can be omitted without losing the reliability of the obtained results. Therefore, to avoid unnecessary involvement of already complex expressions we here apply their soft-gluon equivalents.

The analytical expression for the single gluon radiation spectrum reads [27,30,35,36]

$$\frac{dN_{\text{rad}}}{dx d\tau} = \frac{C_2(G)C_R}{\pi} \frac{1}{x} \int \frac{d^2\mathbf{q}}{\pi} \frac{d^2\mathbf{k}}{\pi} \frac{\mu_E^2(T) - \mu_M^2(T)}{[\mathbf{q}^2 + \mu_E^2(T)][\mathbf{q}^2 + \mu_M^2(T)]} T \alpha_s(ET) \alpha_s \left(\frac{\mathbf{k}^2 + \chi(T)}{x} \right) \times \left[1 - \cos \left(\frac{(\mathbf{k} + \mathbf{q})^2 + \chi(T)}{xE^+} \tau \right) \right] \frac{2(\mathbf{k} + \mathbf{q})}{(\mathbf{k} + \mathbf{q})^2 + \chi(T)} \left[\frac{\mathbf{k} + \mathbf{q}}{(\mathbf{k} + \mathbf{q})^2 + \chi(T)} - \frac{\mathbf{k}}{\mathbf{k}^2 + \chi(T)} \right], \quad (1)$$

where \mathbf{k} and \mathbf{q} denote transverse momenta of radiated and exchanged gluons, respectively; $C_2(G) = 3$ and $C_R = 4/3$ ($C_R = 3$) for the quark (gluon) jet; while $\mu_E(T)$ and $\mu_M(T)$ are electric (Debye) and magnetic screening masses, respectively. The temperature-dependent Debye mass [27,38] is obtained by self-consistently solving Eq. (5) from Ref. [27]. α_s is the (temperature-dependent) running coupling [27,36,39], E is

the initial parton energy, while $\chi(T) = M^2 x^2 + m_g^2(T)$, where x is the longitudinal momentum fraction of the initial parton carried away by the emitted gluon. M is the mass of the propagating parton, while the gluon mass is considered to be equal to its asymptotical mass $m_g = \mu_E/\sqrt{2}$ [40].

The analytical expression for collisional energy loss per unit length is given by the following expression [27,32]:

$$\frac{dE_{\text{coll}}}{d\tau} = \frac{2C_R}{\pi v^2} \alpha_s(ET) \alpha_s(\mu_E^2(T)) \int_0^\infty n_{\text{eq}}(|\vec{\mathbf{k}}|, T) d|\vec{\mathbf{k}}| \times \left[\int_0^{|\vec{\mathbf{k}}|/(1+v)} d|\vec{\mathbf{q}}| \int_{-v|\vec{\mathbf{q}}|}^{v|\vec{\mathbf{q}}|} \omega d\omega + \int_{|\vec{\mathbf{k}}|/(1+v)}^{|\vec{\mathbf{q}}|_{\text{max}}} d|\vec{\mathbf{q}}| \int_{|\vec{\mathbf{q}}|-2|\vec{\mathbf{k}}|}^{v|\vec{\mathbf{q}}|} \omega d\omega \right] \times \left[|\Delta_L(q, T)|^2 \frac{(2|\vec{\mathbf{k}}| + \omega)^2 - |\vec{\mathbf{q}}|^2}{2} + |\Delta_T(q, T)|^2 \frac{(|\vec{\mathbf{q}}|^2 - \omega^2)[(2|\vec{\mathbf{k}}| + \omega)^2 + |\vec{\mathbf{q}}|^2]}{4|\vec{\mathbf{q}}|^4} (v^2|\vec{\mathbf{q}}|^2 - \omega^2) \right], \quad (2)$$

where $n_{\text{eq}}(|\vec{\mathbf{k}}|, T) = \frac{N}{e^{|\vec{\mathbf{k}}|/T-1}} + \frac{N_f}{e^{|\vec{\mathbf{k}}|/T+1}}$ is the equilibrium momentum distribution [22] including gluons, quarks, and antiquarks. k is the four-momentum of the incoming medium parton, v is the velocity of the initial jet, and $q = (\omega, \vec{\mathbf{q}})$ is the four-momentum of the exchanged gluon. $|\vec{\mathbf{q}}|_{\text{max}}$ is provided in Ref. [32], while $\Delta_T(q, T)$ and $\Delta_L(q, T)$ are effective transverse and longitudinal gluon propagators given by Eqs. (3) and (4) from Ref. [27].

Despite the very complicated temperature dependence of Eqs. (1) and (2), in Ref. [29] it was obtained that our dynamical energy-loss formalism [36] (which accommodates

some unique jet-medium effects mentioned above) has an exceptional feature of near linear T dependence. That is, while T^3 dependence for radiative energy loss is widely used [9–12,14–20], from Eq. (1) it is evident that this simplified relation is reproduced with approximations using vacuum gluon propagators (leading to the absence of $m_g(T)$ from the χ expression) and neglecting running coupling. It is straightforward to show that in that case leading T dependence is $\frac{\Delta E_{\text{rad}}}{E} \propto \mu_E^2 T \propto T^3$ ($\mu_E \propto T$). However, Eq. (1) clearly demonstrates that a more realistic T dependence is far from cubic, where in Ref. [29] it was shown that asymptotic T dependence

of our full radiative energy loss is between linear and quadratic.

Additionally, commonly overlooked (due to being smaller compared to radiative at high p_{\perp}) collisional energy loss must not be neglected in suppression predictions [41]. Moreover, widely used dominant T^2 dependence of collisional energy loss [7,21–23] can also be shown to be a consequence of (i) using tree-level diagrams, and consequently introducing artificial cutoffs to nonphysically regulate ultraviolet (and infrared) divergencies (e.g., in Ref. [7]) in the hard momentum transfer sector [22]; or (ii) considering only soft momentum exchange [21]. That is, it is straightforward to show that Eq. (2) recovers leading T^2 dependence from Ref. [21] if (1) only the soft gluon sector is considered, with the upper limit of integration artificially set to $|\vec{q}|_{\max}$; (2) only forward emission is accounted for ($\omega > 0$); and (3) running coupling is neglected. Accordingly, in Ref. [29] it was demonstrated that complex T dependence of our *collisional energy loss* (Eq. (2)) reduces not to commonly considered quadratic, but rather to nearly linear dependence for asymptotically large p_{\perp} . Therefore, a state-of-the-art energy-loss model leads to a much slower growth of the energy loss with temperature compared to the common paradigm, where the widely assumed faster growth can be reproduced only through quite drastic simplifying assumptions.

Since the goal of this paper is the extraction of the temperature-dependence exponent of the energy loss, this paper will furthermore provide an opportunity to test our dynamical energy-loss formalism on a more basic level.

III. NUMERICAL FRAMEWORK

In this paper, the predictions are generated within our fully optimized DREENA [27,28] numerical framework, comprising (i) initial parton momentum distribution [42]; (ii) energy-loss probability based on our dynamical energy-loss formalism [30–32] (discussed in the previous section), which includes multigluon [43] and path-length fluctuations [44], where the path-length fluctuations are calculated according to the procedure provided in Ref. [45] (see also Ref. [28]); and (iii) fragmentation functions [46]. In this paper, we will primarily use two implementations of this framework: (i) DREENA-C, where C corresponds to constant temperature medium; and (ii) DREENA-B, where B corresponds to one-dimensional (1D) Bjorken QGP evolution [7].

In the first part of our paper, using the DREENA-C framework, the average temperature is obtained according to the procedure described in Refs. [28,47], which we briefly outline here. For each centrality region in 5.02-TeV Pb + Pb collisions, the average temperature is estimated through $T^3 \sim \frac{dN_g}{dy} \frac{1}{A_{\perp} L}$ [12,48], where A_{\perp} is the overlap area. $\frac{dN_g}{dy}$ is gluon rapidity density, and is shown to be directly proportional to charged particle multiplicity $\frac{dN_{ch}}{d\eta}$, which is measured for all relevant centralities in 5.02-TeV Pb + Pb collisions at the LHC [49]. Thus, the required expression reads $T = c \left(\frac{dN_{ch}}{A_{\perp} L} \right)^{\frac{1}{3}}$, where constant c can be fixed by effective temperature for 0–20% 2.76-TeV Pb+Pb collisions at LHC [50], leading to, e.g., the average medium temperature of 348 MeV [47,50] in most central 5.02-TeV Pb + Pb collisions at the LHC.

In the second part of this paper, where we use the DREENA-B framework to test the sensitivity of the obtained results, the initial temperature (T_0) for each centrality is estimated in accordance with Ref. [27]. That is, for each centrality class, T_0 is determined in accordance with $T_0 \sim \left(\frac{dN_{ch}}{A_{\perp} L} \right)^{\frac{1}{3}}$ [51]. As a starting point, $T_0 = 500$ MeV in most central 5.02-TeV Pb + Pb collisions at the LHC is estimated from the average medium temperature of 348 MeV [47,50] in these collisions (see above), and a QCD transition temperature of $T_c \approx 155$ MeV [52]. By knowing T_0 in the most central 5.02-TeV Pb + Pb collision, based on the expression above, it is straightforward to obtain T_0 s for different centralities. In both studies, the average path lengths (L) for different centrality classes have been calculated by integrating the path-length distributions [28] which were obtained by following the procedure outlined in Ref. [45], with an additional hard-sphere restriction $r < R_A$ in the Woods-Saxon nuclear density distribution to regulate the path lengths in the peripheral collisions.

In generating numerical predictions, all the parameters correspond to standard literature values, i.e., we use no fitting parameters. We consider a QGP with $n_f = 3$ and $\Lambda_{\text{QCD}} = 0.2$ GeV. For the light quarks we assume that their mass is dominated by the thermal mass $M \approx \mu_E / \sqrt{6}$. The magnetic to electric mass ratio is assumed to be $0.4 < \mu_M / \mu_E < 0.6$ [53,54].

IV. RESULTS AND DISCUSSION

In this section, we first address the choice of the suitable observable for extracting energy-loss temperature dependence. For this purpose, an observable which is sensitive only to the details of jet-medium interactions (to facilitate extraction of T dependence), rather than the subtleties of medium evolution (to avoid unnecessary complications and ensure robustness), would be optimal. R_{AA} has such features, since it was previously reported that it is very sensitive to energy-loss effects [41] and the average medium properties, while being practically insensitive to the details of medium evolution (as opposed to v_2) [26–28,55,56]. Therefore, it is plausible that the appropriate observable should be closely related to R_{AA} .

Our theoretical and numerical approaches described above (where the dynamical energy loss explicitly depends on T) are implemented in a fully optimized DREENA framework [27,28], which makes it suitable for this paper. To more easily interpret the obtained results, we start from a constant T medium, i.e., DREENA-C [28]. In this framework, the local temperature becomes the average (constant) temperature—this makes the extraction of the temperature dependence straightforward, which is the main advantage of that framework. To confirm that, through such procedure, we indeed extracted the local temperature dependence, we will use DREENA-B [27] as a crosscheck, as this more complex model incorporates medium evolution through 1D Bjorken longitudinal expansion [7]. We here exploit that DREENA-C and DREENA-B are analytically tractable, allowing us to derive the appropriate scaling behavior. Finally, as a check of sensitivity of our proposed observable to the details of the medium evolution we employ our DREENA-A framework (“A” stands

for “adaptive”), which employs state-of-the-art full three- plus one-dimensional (3+1D) hydrodynamical evolution.

With the intention of extracting simple functional dependence on T (of the otherwise analytically and numerically quite complex dependence of the fractional energy loss; see Eqs. (1) and (2)), we first provide the scaling arguments within the DREENA-C [28] framework. These scaling (analytical) arguments will then be followed by a full-fledged numerical analysis. Namely, in Refs. [26–28,43] it was shown that, at very large values of transverse momentum p_{\perp} and/or in peripheral collisions, the following estimates can be made:

$$\begin{aligned}\Delta E/E &\approx \eta T^a L^b, \\ R_{AA} &\approx 1 - \xi T^a L^b,\end{aligned}\quad (3)$$

where η denotes a proportionality factor, depending on initial parton transverse momentum and its flavor, while $\xi = (n - 2)\eta/2$, where n is the steepness of a power-law fit to the initial transverse momentum distribution, i.e., $d\sigma/dp_{\perp}^2 \propto p_{\perp}^{-n}$. T and L denote the average temperature (of the QCD medium) along the jet path and the average path length traversed by the energetic parton. The scaling factors for temperature and path-length energy-loss dependence are denoted as a and b , respectively.

We next formulate the quantity R_{AA}^T , with the goal to isolate the temperature dependence:

$$R_{AA}^T = \frac{1 - R_{AA}}{1 - R_{AA}^{\text{ref}}}, \quad (4)$$

which presents the $(1 - R_{AA})$ ratio for a pair of two different centrality classes. The centrality class that corresponds to R_{AA}^{ref} (i.e., the quantity in the denominator) is denoted as the referent centrality, and is always lower (corresponding to a more central collision) than centrality in the numerator. We term this new quantity, given by Eq. (4), as a *temperature-dependent suppression ratio* (R_{AA}^T), which we will further elucidate below.

Namely, by using Eq. (3), it is straightforward to isolate average T and average path-length dependence of R_{AA}^T :

$$R_{AA}^T = \frac{1 - R_{AA}}{1 - R_{AA}^{\text{ref}}} \approx \frac{\xi T^a L^b}{\xi T_{\text{ref}}^a L_{\text{ref}}^b} = \left(\frac{T}{T_{\text{ref}}}\right)^a \left(\frac{L}{L_{\text{ref}}}\right)^b, \quad (5)$$

which in logarithmic form reads

$$\ln(R_{AA}^T) = \ln\left(\frac{1 - R_{AA}}{1 - R_{AA}^{\text{ref}}}\right) \approx a \ln\left(\frac{T}{T_{\text{ref}}}\right) + b \ln\left(\frac{L}{L_{\text{ref}}}\right). \quad (6)$$

However, the remaining dependence of the newly defined quantity on the path length is undesired for the purpose of this paper. So, in order to make use of the previous equation, we first test how the two terms on the right-hand side of Eq. (6) are related. To this end, in Fig. 1 we plot $\ln(L/L_{\text{ref}})$ against $\ln(T/T_{\text{ref}})$ for several combinations of centralities, as denoted in the caption of Fig. 1.

Conveniently, Fig. 1 shows a linear dependence $\ln(L/L_{\text{ref}}) \approx k \ln(T/T_{\text{ref}})$, with $k \approx 1.86$. This leads to a simple relation:

$$\ln(R_{AA}^T) \approx (a + kb) \ln\left(\frac{T}{T_{\text{ref}}}\right), \quad (7)$$

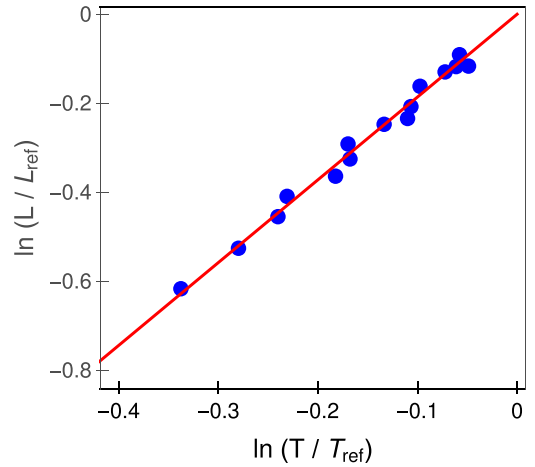


FIG. 1. $\ln(L/L_{\text{ref}})$ vs $\ln(T/T_{\text{ref}})$ in 5.02-TeV Pb+Pb collisions at the LHC for various centrality pairs. The referent centralities (for quantities in denominators) acquire one of the values 5–10, 10–20, 20–30, 30–40, or 40–50%, while the centralities in the numerator are always higher (the highest one being 50–60%). The solid red line corresponds to the linear fit to the calculated points.

so that with $f = a + kb$

$$R_{AA}^T \approx \left(\frac{T}{T_{\text{ref}}}\right)^f, \quad (8)$$

where this simple form facilitates extraction of a .

In Eq. (8), R_{AA}^T depends solely on T and effectively the temperature-dependence exponent a (as k and b [26] are known), which justifies the use of the “temperature-sensitive” term with this new quantity. Therefore, here we propose R_{AA}^T , given by Eq. (4), as a new observable, which is highly suitable for the purpose of this paper. Note, however, that this coupled dependence of R_{AA}^T on a and b exponents has its advantage, since it allows using this new observable to shed light on the underlying energy-loss mechanisms, by differentiating between various energy-loss models on both their T and L dependences.

The proposed extraction method is the following: We use our full-fledged DREENA-C numerical procedure to generate predictions for R_{AA} and thereby for the left-hand side of Eq. (8). Calculation of average T is already outlined in the previous section and described in detail above. We will generate the predictions with a full-fledged procedure, where we expect asymptotic scaling behavior (given by Eq. (8)) to be valid at high $p_{\perp} \approx 100$ GeV. Having in mind that values of k and b parameters have been extracted earlier, the temperature-dependence exponent a in the very high- p_{\perp} limit can then be estimated from the slope (f) of a $\ln(R_{AA}^T)$ vs $\ln(T/T_{\text{ref}})$ linear fit, done for a variety of centrality pairs.

However, before embarking on this task, we first verify whether our predictions of R_{AA}^T for different centrality classes, based on the full-fledged DREENA-C framework, are consistent with the available experimental data. In Fig. 2 we compare our R_{AA}^T vs p_{\perp} predictions for charged hadrons with corresponding 5.02-TeV Pb + Pb LHC data from A Large Ion Collider Experiment (ALICE) [57], Compact Muon Solenoid

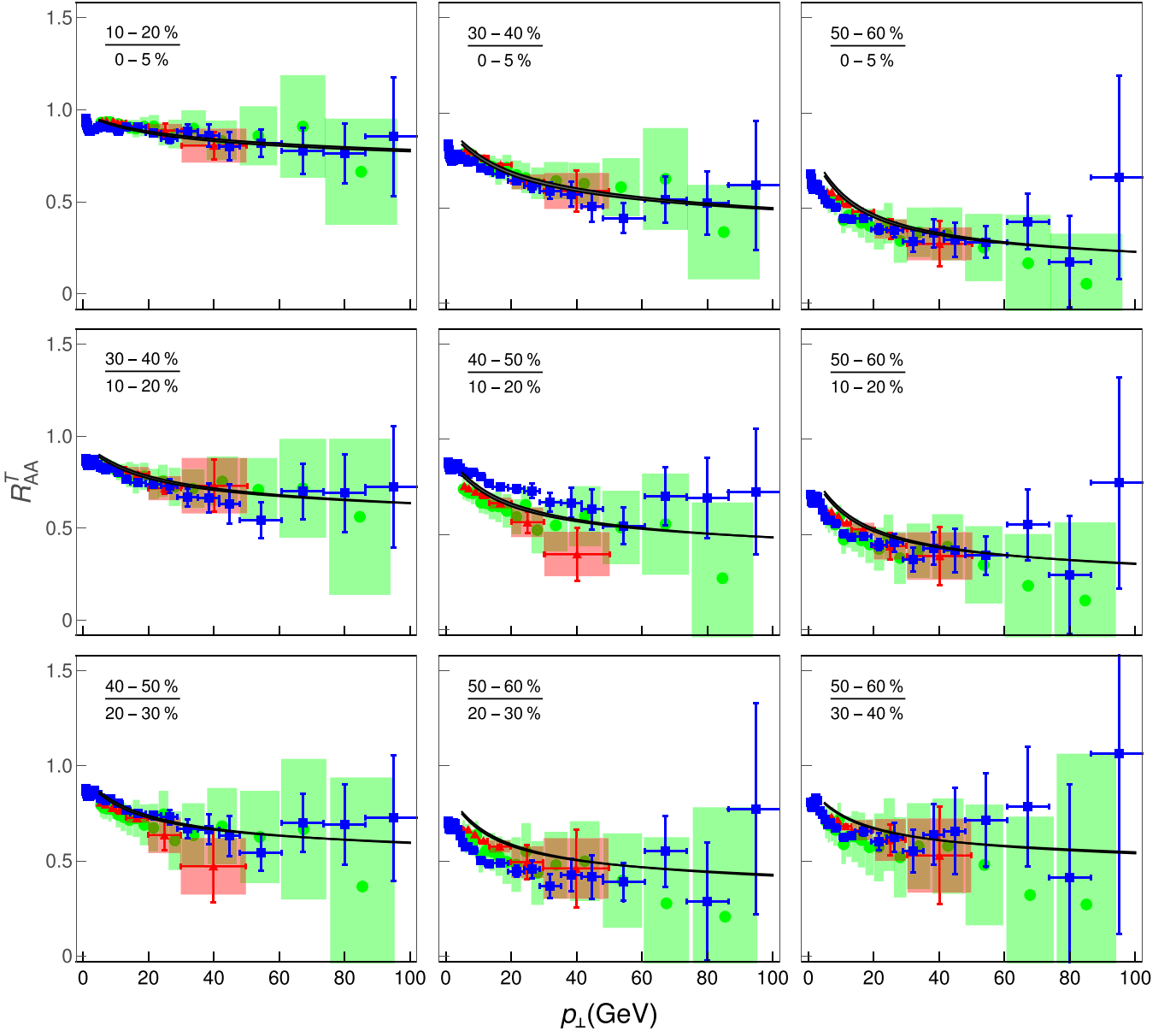


FIG. 2. Charged hadron R_{AA}^T for different pairs of centrality classes as a function of p_{\perp} . The predictions generated within our full-fledged suppression numerical procedure DREENA-C [28] (black curves with corresponding gray bands) are compared with ALICE [57] (red triangles), CMS [58] (blue squares), and ATLAS [59] (green circles) data. The lower (upper) boundary of each band corresponds to $\mu_M/\mu_E = 0.6$ ($\mu_M/\mu_E = 0.4$). Centrality pairs are indicated in the upper-left corner of each plot.

(CMS) [58], and A Toroidal LHC ApparatuS (ATLAS) [59], for different centrality pairs as indicated in the upper-left corner of each plot. Despite the large error bars, for all centrality pairs we observe consistency between our DREENA-C predictions and experimental data, in the p_{\perp} region where our formalism is applicable ($p_{\perp} \gtrsim 10$ GeV). Moreover, we also notice the flattening of each curve with increasing p_{\perp} (≈ 100 GeV), confirming that the expecting saturating (limiting) behavior is reached.

Furthermore, based on the analytical relation provided by Eq. (7), we expect linear functional dependence between $\ln R_{AA}^T$ and $\ln(T/T_{\text{ref}})$, which we test in Fig. 3. Note that all quantities throughout the paper are determined at $p_{\perp} = 100$ GeV, and by calculating R_{AA}^T for various centrality pairs

(see figure captions) within the full-fledged DREENA procedure. Remarkably, from Fig. 3, we observe that $\ln(R_{AA}^T)$ and $\ln(T/T_{\text{ref}})$ are indeed linearly related, which confirms the validity of our scaling arguments at high p_{\perp} and the proposed procedure.

Linear fit to calculated points in Fig. 3 leads to the proportionality factor $f = a + kb = 3.79 \approx 4$. This small value of f would lead to k smaller than 1 if (commonly assumed) $a = 3$ and $b = 2$ are used. Such k value seems, however, implausible, as it would require (T/T_{ref}) to change more slowly with centrality compared to (L/L_{ref}) .

More importantly, the temperature exponent can now be extracted ($b \approx 1.4$ as estimated in Ref. [26]), leading to $a \approx 1.2$. This indicates that temperature dependence of energetic

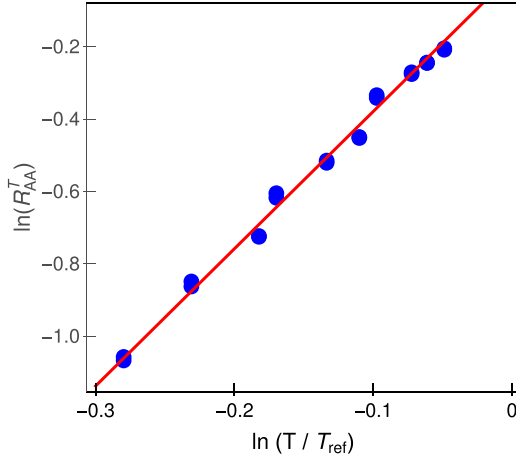


FIG. 3. $\ln(R_{AA}^T)$ vs $\ln(T/T_{\text{ref}})$ relation. $\ln(R_{AA}^T)$ and $\ln(T/T_{\text{ref}})$ are calculated from the full-fledged DREENA-C framework [28], for h^\pm at $p_\perp = 100$ GeV in 5.02-TeV Pb+Pb collisions at the LHC for different centrality pairs. The referent centrality values are 10–20, 20–30, 30–40, and 40–50%, while their counterpart values are always higher, with the highest being equal to 50–60%. The red solid line corresponds to the linear fit to the values. Remaining parameters are the same as in Fig. 2.

particle energy loss (at very high p_\perp) is close to linear (see Eq. (3)), that is, certainly not quadratic or cubic, as commonly considered. This is in accordance with previously reported dependence of fractional dynamical energy loss on T somewhere between linear and quadratic [29], and as opposed to commonly used pQCD estimate $a = 3$ for radiative [9–12,14–20] (or even $a = 2$ for collisional [7,21–23]) energy loss.

The extraction of T dependence, together with previously estimated path-length dependence [26], within the DREENA framework, allows utilizing this new observable R_{AA}^T in discriminating between energy-loss models, with the aim of better understanding QGP properties. To this end, in Fig. 4, we (i) test sensitivity of R_{AA}^T on different medium evolutions (constant temperature, 1D Bjorken [60], and full 3+1D hydrodynamics [61]) and (ii) compare the asymptote derived from this study ($(T/T_{\text{ref}})^{1.2}(L/L_{\text{ref}})^{1.4}$), with the commonly used estimate of $(T/T_{\text{ref}})^3(L/L_{\text{ref}})^2$.

Several conclusions can be drawn from Fig. 4.

(i) With respect to different models of QGP expansion, we see that, as expected, obtained R_{AA}^T results are similar, i.e., not very sensitive to the details of the medium evolution. As in DREENA-C (and DREENA-B; see the next subsection) the temperature dependence can be analytically tracked (which is, however, not possible in more complex DREENA-A), this result additionally confirms that the DREENA-C framework is suitable for the extraction of energy-loss temperature dependence.

(ii) Ideally, the T dependence exponent could be directly extracted from experimental data, by fitting a straight line to the very high- p_\perp part (≈ 100 GeV) of R_{AA}^T for practically any centrality pair (upon L the dependence exponent is determined following Ref. [26]). However, the fact that data from different experiments (ALICE, CMS, and ATLAS) are not ideally consistent, and that the error bars are quite sizable,

currently prevents such direct extraction. The error bars in the upcoming high-luminosity third run at the LHC are, however, expected to significantly decrease, which would enable the direct extraction of the exponent a from the data.

(iii) Finally, Fig. 4 also indicates that widely considered energy-loss dependence T^3L^2 may be inconsistent with the experimental data. Future increase in measurements precision could provide confidence in this observation and resolve the exact form of these dependencies from the data, through our proposed observable. This discriminative power of the R_{AA}^T quantity highlights its importance in understanding the underlying energy-loss mechanisms in QGP.

A. Effects of medium evolution

While in Fig. 4 we showed that R_{AA}^T results are robust with respect to the medium evolution, the analytical procedure for extracting temperature dependence is different in DREENA-C and DREENA-B frameworks. A comparison of scaling factors extracted from these two procedures can be used to test reliability of the proposed procedure. In this subsection, we consequently utilize the DREENA-B framework [27], where medium evolution is introduced through Bjorken 1D hydrodynamical expansion [60], i.e., there is the following functional dependence of T on path length:

$$T = T_0 \left(\frac{\tau_0}{l} \right)^{1/3}, \quad (9)$$

where T_0 and $\tau_0 = 0.6$ fm [62,63] denote initial temperature and thermalization time of the QGP.

Proceeding in a similar manner as in constant medium case, R_{AA}^T (given by Eq. (4)) in the evolving medium (for coupled local T and l , where l stands for traversed path length) reads

$$\begin{aligned} R_{AA}^T &= \frac{\int_0^L T^a l^{b-1} dl}{\int_0^{L_{\text{ref}}} (T_{\text{ref}})^a (l_{\text{ref}})^{b-1} dl_{\text{ref}}} = \frac{T_0^a \tau_0^{a/3} \int_0^L \frac{l^{b-1}}{l^{a/3}} dl}{T_{0,\text{ref}}^a \tau_0^{a/3} \int_0^{L_{\text{ref}}} \frac{(l_{\text{ref}})^{b-1}}{(l_{\text{ref}})^{a/3}} dl_{\text{ref}}} \\ &= \left(\frac{T_0}{T_{0,\text{ref}}} \right)^a \left(\frac{L}{L_{\text{ref}}} \right)^{b-\frac{a}{3}}, \end{aligned} \quad (10)$$

where we used Eq. (9). Again, we assess whether there is a simple relation between logarithms of the (now initial) temperature ratio and average path-length ratio for different centrality pairs. Similarly to the constant T case, from Fig. 5 we infer linear dependence between these two quantities, where the slope coefficient now acquires the value $\kappa \approx 1.3$. Thus, we may write

$$\frac{L}{L_{\text{ref}}} = \left(\frac{T_0}{T_{0,\text{ref}}} \right)^\kappa \Rightarrow \frac{T_0}{T_{0,\text{ref}}} = \left(\frac{L}{L_{\text{ref}}} \right)^{1/\kappa}, \quad (11)$$

which ensures that the R_{AA}^T quantity has a very simple form, depending only on average path length and exponents a , b , and κ :

$$R_{AA}^T = \left(\frac{L}{L_{\text{ref}}} \right)^{\frac{a}{\kappa} + b - \frac{a}{3}}. \quad (12)$$

If we substitute the value of $a \approx 1.2$ obtained in the constant T medium case, previously estimated $b \approx 1.4$ [26], and

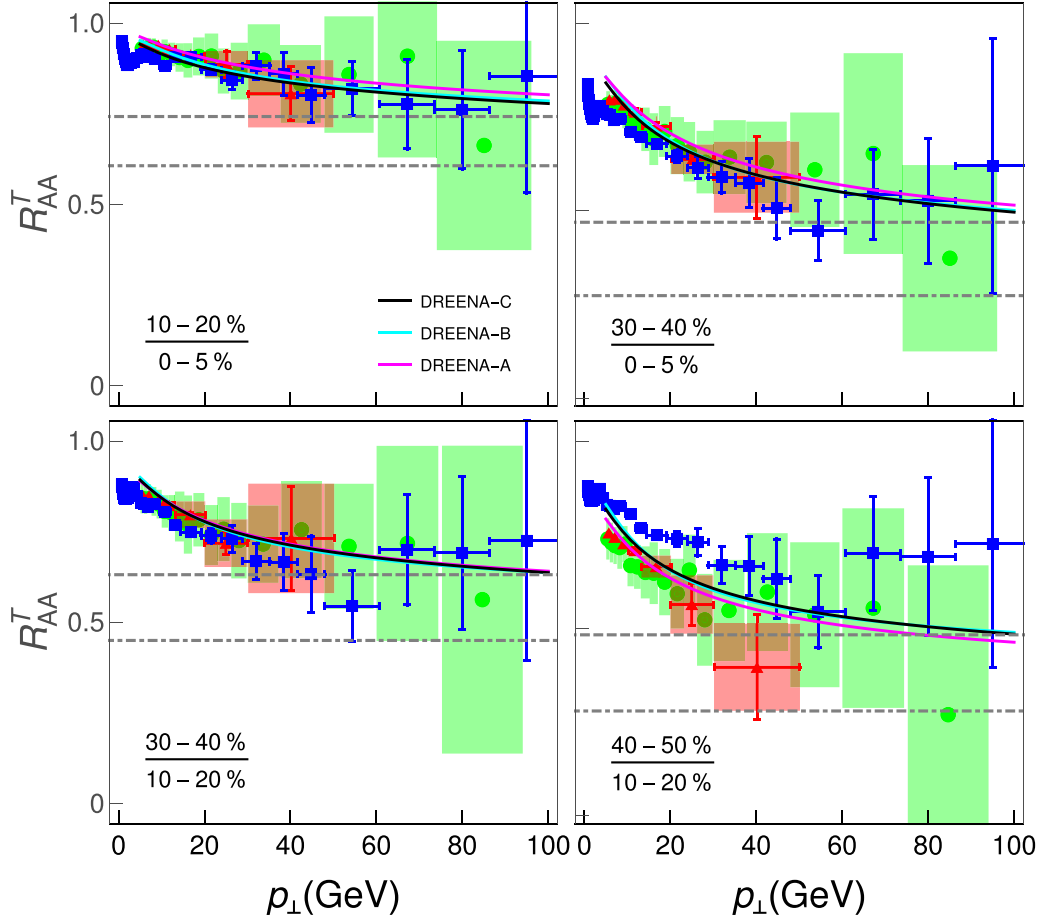


FIG. 4. The discriminative power of the R_{AA}^T quantity in resolving the energy-loss mechanism. Four panels in Fig. 2 are extended to include comparison of our asymptotic scaling behavior $(T/T_{\text{ref}})^{1.2}(L/L_{\text{ref}})^{1.4}$ (gray dashed horizontal line) with common assumption $(T/T_{\text{ref}})^3(L/L_{\text{ref}})^2$ (gray dot-dashed horizontal line). The figure also shows comparison of R_{AA}^T s obtained by three different numerical frameworks: constant temperature DREENA-C (black curve), 1D Bjorken expansion DREENA-B [27] (cyan curve), and full 3+1D hydrodynamics evolution [61] DREENA-A (magenta curve). The remaining labeling is the same as in Fig. 2.

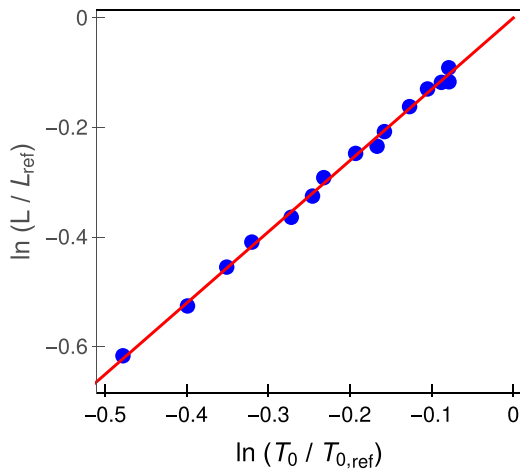


FIG. 5. $\ln(L/L_{\text{ref}})$ vs $\ln(T_0/T_{0,\text{ref}})$ for various pairs of centralities in evolving medium. The assumed centrality pairs are the same as in Fig. 1. The red solid line corresponds to the linear fit to the values.

here inferred $\kappa \approx 1.3$, we arrive at the following estimate:

$$R_{AA}^T = \left(\frac{L}{L_{\text{ref}}}\right)^{1.93} \Rightarrow \ln(R_{AA}^T) = 1.93 \ln\left(\frac{L}{L_{\text{ref}}}\right). \quad (13)$$

This equation is quite suitable for testing the robustness of the procedure for extracting the exponent a to inclusion of the evolving medium. Namely, value 1.93 in Eq. (13) stems from coefficient a , which is extracted from the constant T medium case. On the other hand, if we plot $\ln(R_{AA}^T)$, generated by full-fledged DREENA-B calculations (i.e., in the evolving medium) which are *fundamentally different* from DREENA-C, against $\ln(L/L_{\text{ref}})$ for a variety of centrality pairs, again we observe a linear dependence (see Fig. 6). Furthermore, a linear fit to the values surprisingly yields the exact same slope coefficient value of 1.93 (see also Table I).

Consequently, the procedure of extracting the temperature-dependence exponent, introduced first in the case of the constant T medium, is applicable to the expanding medium as well. Moreover, the fact that the same coefficient a is obtained through two different procedures leads us to conclude that (i) for the purpose of this paper the DREENA-C framework

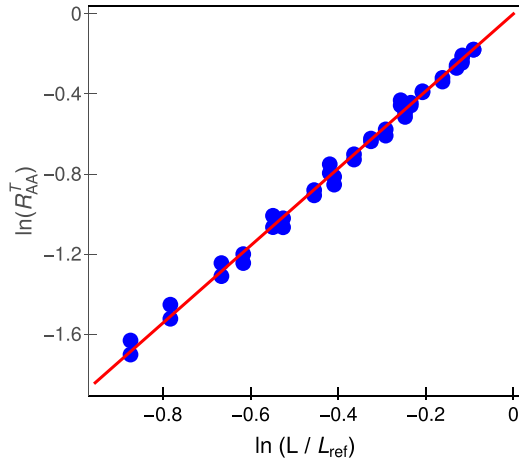


FIG. 6. Testing the validity of our procedure for temperature-dependence extraction in the case of the expanding QCD medium. $\ln(R_{AA}^T)$ vs $\ln(L/L_{\text{ref}})$ for h^\pm at $p_\perp = 100$ GeV for different pairs of centrality classes is plotted. Suppression predictions are obtained from full-fledged DREENA-B [27] calculations. Referent centrality values are 5–10, 10–20, 20–30, 30–40, 40–50, and 50–60%, while their counterpart values are always higher, with the highest being 60–70%. The red solid line corresponds to the linear fit to the values.

(assuming a constant temperature medium) is sufficient and (ii) the same energy-loss scaling holds in an evolving medium (i.e., for local temperature) as well. The displayed consistency of the results provides confidence in the general applicability of our procedure (suggesting robustness to the applied model of the bulk medium) and supports the reliability of the value of extracted T dependence exponent $a \approx 1.2$.

It is worth noting that the definition of R_{AA}^T relies on the fact that we assume that $R_{AA} = 1$ if no energy loss is encountered. Related to this, we do not study the effect of (nuclear) parton distribution function differences on R_{AA} , as it is generally studied under initial-state effects. However, it is known that initial-state effects have a sizable impact only on the low- and moderate- p_\perp sector (lower than 6 GeV) [64–70]. Since our numerical predictions are generated above 8–10 GeV and the temperature dependence is extracted at very high- p_\perp values ($p_\perp \sim 100$ GeV), these effects will be negligible in this p_\perp region, and should not influence the results obtained in our paper.

B. Effects of colliding system size

We below extend our analysis to smaller colliding systems in order to assess generality of the conclusions presented

TABLE I. Inferred temperature-dependence exponent across different frameworks.

Framework	Temperature dependence exponent
DREENA-C	$a \approx 1.2$
DREENA-B	Consistent with $a \approx 1.2$
DREENA-A	Not analytically tractable

above. Smaller colliding systems, such as Xe + Xe, Kr + Kr, Ar + Ar, and O + O, are important to gradually resolve the issue of QGP formation in small systems (such as pA), and (except Xe + Xe, which is already in a run) are expected to be a part of the future heavy-ion program at the LHC [71].

As already discussed in Ref. [26], for this analysis within the DREENA-C framework [28] (which we employ here for simplicity, since the robustness of the procedure to the evolving medium was demonstrated above) note that R_{AA} depends on (i) initial high- p_\perp parton distribution, (ii) medium average T , and (iii) path-length distribution. For different colliding systems (probably at slightly different $\sqrt{s_{NN}} = 5.44$ TeV compared to the Pb + Pb system) we employ the same high- p_\perp distributions, since in Ref. [29] it was shown that for almost twofold increase of the collision energy (from 2.76 to 5.02 TeV) the change in corresponding initial distributions results in a negligible change (approximately 5%) in suppression.

Regarding the average temperature, one should note that T is directly proportional to the charged particle multiplicity, while inversely proportional to the size of the overlap area and average medium size [26,28,47,48], i.e., $T \propto (\frac{dN_{ch}/d\eta}{A_\perp L})^{1/3}$. The transition to smaller colliding systems, for a certain fixed centrality class, leads to the following scaling: $A_\perp \propto A^{2/3}$, $L \propto A^{1/3}$ [72,73], and $dN_{ch}/d\eta \propto N_{\text{part}} \propto A$ [74,75], where A denotes atomic mass. This leads to $T \sim (\frac{A}{A_\perp^3 L})^{1/3} \sim \text{const}$, that is, we expect that average temperature does not change, when transitioning from large Pb + Pb to smaller systems, for a fixed centrality class. Lastly, path-length distributions for smaller systems and each centrality class are obtained in the same manner as for Pb+Pb [28], and are the same as in Pb + Pb collisions up to a rescaling factor of $A^{1/3}$.

By denoting all quantities related to smaller systems with a tilde, with Pb + Pb quantities denoted as before, it is straightforward to show that the temperature sensitive suppression ratio for smaller systems satisfies

$$\begin{aligned} \tilde{R}_{AA}^T &= \frac{1 - \tilde{R}_{AA}}{1 - R_{AA}^{\text{ref}}} \approx \frac{\tilde{T}^a \tilde{L}^b}{T_{\text{ref}}^a L_{\text{ref}}^b} \approx \frac{T^a L^b (\tilde{A}/A)^{b/3}}{T_{\text{ref}}^a L_{\text{ref}}^b (\tilde{A}/A)^{b/3}} \\ &= \frac{1 - R_{AA}}{1 - R_{AA}^{\text{ref}}} = R_{AA}^T, \end{aligned} \quad (14)$$

where we used $\tilde{T} = T$ and $\tilde{L}/L = (\tilde{A}/A)^{1/3}$.

To validate equality of R_{AA}^T s for different system sizes, predicted by analytical scaling behavior (Eq. (14)), in Fig. 7 we compare our full-fledged R_{AA}^T predictions for h^\pm in the Pb + Pb system with those for smaller colliding systems. We observe that, practically irrespective of system size, R_{AA}^T exhibits the same asymptotical behavior at high p_\perp . This not only validates our scaling arguments, but also demonstrates the robustness of the new observable R_{AA}^T to system size. Consequently, since for fixed centrality range T should remain the same for all these colliding systems, we obtained that temperature-dependence exponent a should be the same independently of the considered colliding system (see Fig. 3). Therefore, the proposed procedure for extracting the

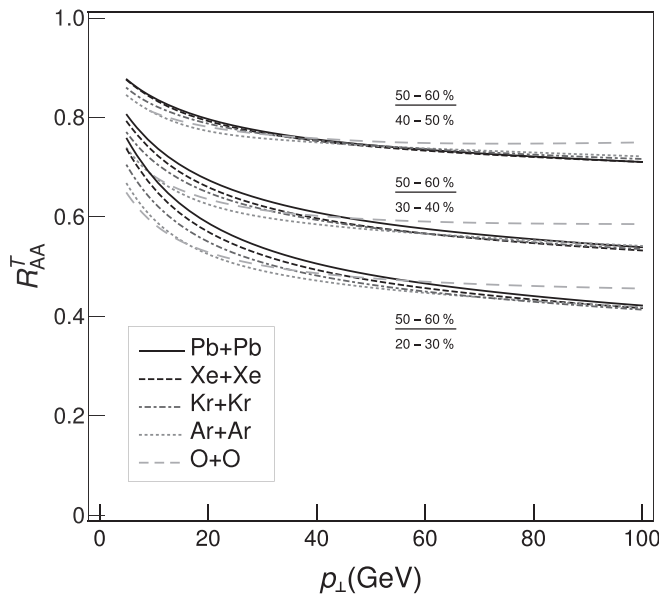


FIG. 7. Dependence of R_{AA}^T on a system size as a function of p_{\perp} . Predictions for h^{\pm} generated within the full-fledged DREENA-C [28] suppression numerical procedure are compared for different colliding systems: Pb+Pb, Xe + Xe, Kr + Kr, Ar + Ar, and O + O (for lines specification see legend). For clarity, the results are shown only for three centrality pairs, as specified in the plot, although checked for all available centrality classes. The magnetic to electric mass ratio is fixed to $\mu_M/\mu_E = 0.4$.

temperature dependence of the energy loss is also robust to the collision system size. As a small exception, the O + O system exhibits a slight departure from the remaining systems at high p_{\perp} , which might be a consequence of the fact that this system is significantly smaller than other systems considered here.

V. CONCLUSIONS AND OUTLOOK

One of the main signatures of the high- p_{\perp} particle's energy loss, apart from its path length, is its temperature dependence. Although extensive studies on both issues were performed, not until recently was the path-length dependence resolution suggested [26]. Here we proposed a new simple observable for extracting temperature dependence of the energy loss, based on one of the most common jet quenching observables—the high- p_{\perp} suppression. By combining full-fledged numerical calculations with asymptotic scaling behavior, we surprisingly obtained that temperature dependence is nearly linear, i.e., far from quadratic or cubic, as commonly assumed. Further, we verified its robustness and reliability on colliding system size and evolving QGP medium. Moreover, we demonstrated that the same observable, due to its joint dependence on T and L exponents, can be utilized to discriminate between different energy-loss models on *both* their *temperature* and *path-length* dependence bases. Comparison with the experimental data also indicated a need for revising the long-standing $\Delta E/E \propto L^2 T^3$ paradigm.

As an outlook, the expected substantial decrease of error bars in the upcoming third run measurements at the LHC will allow direct extraction of the temperature-dependence exponent from high- p_{\perp} data of this observable. This will provide a resolving power to temperature/path-length [26] dependence of the energy loss and test our understanding of the underlying QGP physics.

ACKNOWLEDGMENTS

We thank Pasi Huovinen and Jussi Auvinen for useful discussions. This work is supported by the European Research Council (Grant No. ERC-2016-COG: 725741), and by the Ministry of Science and Technological Development of the Republic of Serbia (Projects No. ON171004 and No. ON173052).

- [1] M. Gyulassy and L. McLerran, *Nucl. Phys. A* **750**, 30 (2005).
- [2] E. V. Shuryak, *Nucl. Phys. A* **750**, 64 (2005).
- [3] C. V. Johnson and P. Steinberg, *Phys. Today* **63**(5), 29 (2010).
- [4] B. Jacak and P. Steinberg, *Phys. Today* **63**(5), 39 (2010).
- [5] J. C. Collins and M. J. Perry, *Phys. Rev. Lett.* **34**, 1353 (1975).
- [6] G. Baym and S. A. Chin, *Phys. Lett. B* **62**, 241 (1976).
- [7] J. D. Bjorken, FERMILAB-PUB-82-059-THY, 287 (1982).
- [8] J. Adams *et al.* (STAR Collaboration), *Phys. Rev. Lett.* **91**, 072304 (2003); C. Adler *et al.* (STAR Collaboration), *ibid.* **90**, 082302 (2003).
- [9] R. Baier, Y. Dokshitzer, A. Mueller, S. Peigne, and D. Schiff, *Nucl. Phys. B* **484**, 265 (1997).
- [10] N. Armesto, C. A. Salgado, and U. A. Wiedemann, *Phys. Rev. D* **69**, 114003 (2004).
- [11] C. A. Salgado and U. A. Wiedemann, *Phys. Rev. D* **68**, 014008 (2003).
- [12] M. Gyulassy, P. Levai, and I. Vitev, *Nucl. Phys. B* **594**, 371 (2001).
- [13] B. G. Zakharov, *JETP Lett.* **70**, 176 (1999); **73**, 49 (2001).
- [14] P. B. Arnold, G. D. Moore, and L. G. Yaffe, *J. High Energy Phys.* **06** (2002) 030.
- [15] X. N. Wang and X. F. Guo, *Nucl. Phys. A* **696**, 788 (2001).
- [16] C. Andres, N. Armesto, M. Luzum, C. A. Salgado, and P. Zurita, *Eur. Phys. J. C* **76**, 475 (2016).
- [17] B. Betz and M. Gyulassy, *Phys. Rev. C* **86**, 024903 (2012).
- [18] B. Betz and M. Gyulassy, *J. High Energy Phys.* **08** (2014) 090; **10** (2014) 043.
- [19] J. Noronha-Hostler, B. Betz, J. Noronha, and M. Gyulassy, *Phys. Rev. Lett.* **116**, 252301 (2016).
- [20] A. Majumder and C. Shen, *Phys. Rev. Lett.* **109**, 202301 (2012).
- [21] M. H. Thoma and M. Gyulassy, *Nucl. Phys. B* **351**, 491 (1991).
- [22] E. Braaten and M. H. Thoma, *Phys. Rev. D* **44**, 1298 (1991); **44**, 2625(R) (1991).
- [23] Y. He, T. Luo, X.-N. Wang, and Y. Zhu, *Phys. Rev. C* **91**, 054908 (2015); **97**, 019902(E) (2018).
- [24] C. Nonaka and S. A. Bass, *Phys. Rev. C* **75**, 014902 (2007).
- [25] C. Marquet and T. Renk, *Phys. Lett. B* **685**, 270 (2010).
- [26] M. Djordjevic, D. Zigic, M. Djordjevic, and J. Auvinen, *Phys. Rev. C* **99**, 061902(R) (2019).

- [27] D. Zigic, I. Salom, M. Djordjevic, and M. Djordjevic, *Phys. Lett. B* **791**, 236 (2019).
- [28] D. Zigic, I. Salom, J. Auvinen, M. Djordjevic, and M. Djordjevic, *J. Phys. G* **46**, 085101 (2019).
- [29] M. Djordjevic and M. Djordjevic, *Phys. Rev. C* **92**, 024918 (2015).
- [30] M. Djordjevic, *Phys. Rev. C* **80**, 064909 (2009).
- [31] M. Djordjevic and U. Heinz, *Phys. Rev. Lett.* **101**, 022302 (2008).
- [32] M. Djordjevic, *Phys. Rev. C* **74**, 064907 (2006).
- [33] J. I. Kapusta, *Finite-Temperature Field Theory* (Cambridge University, Cambridge, England, 1989).
- [34] M. Djordjevic and M. Gyulassy, *Nucl. Phys. A* **733**, 265 (2004).
- [35] M. Djordjevic, *Phys. Lett. B* **709**, 229 (2012).
- [36] M. Djordjevic and M. Djordjevic, *Phys. Lett. B* **734**, 286 (2014).
- [37] B. Blagojevic, M. Djordjevic, and M. Djordjevic, *Phys. Rev. C* **99**, 024901 (2019).
- [38] A. Peshier, [arXiv:hep-ph/0601119](https://arxiv.org/abs/hep-ph/0601119).
- [39] R. Field, *Applications of Perturbative QCD* (Perseus, Cambridge, MA, 1995).
- [40] M. Djordjevic and M. Gyulassy, *Phys. Rev. C* **68**, 034914 (2003).
- [41] B. Blagojevic and M. Djordjevic, *J. Phys. G* **42**, 075105 (2015).
- [42] Z. B. Kang, I. Vitev, and H. Xing, *Phys. Lett. B* **718**, 482 (2012); R. Sharma, I. Vitev, and B. W. Zhang, *Phys. Rev. C* **80**, 054902 (2009).
- [43] M. Gyulassy, P. Levai, and I. Vitev, *Phys. Lett. B* **538**, 282 (2002).
- [44] S. Wicks, W. Horowitz, M. Djordjevic, and M. Gyulassy, *Nucl. Phys. A* **784**, 426 (2007).
- [45] A. Dainese, *Eur. Phys. J. C* **33**, 495 (2004).
- [46] D. de Florian, R. Sassot, and M. Stratmann, *Phys. Rev. D* **75**, 114010 (2007).
- [47] M. Djordjevic, M. Djordjevic, and B. Blagojevic, *Phys. Lett. B* **737**, 298 (2014).
- [48] J. Xu, A. Buzzatti, and M. Gyulassy, *J. High Energy Phys.* **08** (2014) 063.
- [49] J. Adam *et al.* (ALICE Collaboration), *Phys. Rev. Lett.* **116**, 222302 (2016).
- [50] J. Adam *et al.* (ALICE Collaboration), *Phys. Lett. B* **754**, 235 (2016); M. Wilde (for the ALICE Collaboration), *Nucl. Phys. A* **904-905**, 573c (2013).
- [51] M. Djordjevic, M. Gyulassy, R. Vogt, and S. Wicks, *Phys. Lett. B* **632**, 81 (2006).
- [52] A. Bazavov *et al.* (HotQCD Collaboration), *Phys. Rev. D* **90**, 094503 (2014).
- [53] Y. Maezawa, S. Aoki, S. Ejiri, T. Hatsuda, N. Ishii, K. Kanaya, N. Ukita, and T. Umeda (WHOT-QCD Collaboration), *Phys. Rev. D* **81**, 091501(R) (2010).
- [54] A. Nakamura, T. Saito, and S. Sakai, *Phys. Rev. D* **69**, 014506 (2004).
- [55] T. Renk, *Phys. Rev. C* **85**, 044903 (2012).
- [56] D. Molnar and D. Sun, *Nucl. Phys. A* **932**, 140 (2014); **910-911**, 486 (2013).
- [57] S. Acharya *et al.* (ALICE Collaboration), *J. High Energy Phys.* **11** (2018) 013.
- [58] V. Khachatryan *et al.* (CMS Collaboration), *J. High Energy Phys.* **04** (2017) 039.
- [59] (ATLAS Collaboration), ATLAS-CONF-2017-012 (2017).
- [60] J. D. Bjorken, *Phys. Rev. D* **27**, 140 (1983).
- [61] E. Molnar, H. Holopainen, P. Huovinen, and H. Niemi, *Phys. Rev. C* **90**, 044904 (2014).
- [62] P. F. Kolb and U. W. Heinz, Hydrodynamic description of ultra-relativistic heavy ion collisions, in *Quark-Gluon Plasma*, edited by R. C. Hwa and X.-N. Wang (World Scientific, Singapore, 2004), Vol. 3, p. 634.
- [63] J. E. Bernhard, J. S. Moreland, and S. A. Bass, *Nucl. Phys. A* **967**, 293 (2017).
- [64] M. R. Adams *et al.*, *Phys. Rev. Lett.* **68**, 3266 (1992).
- [65] V. Barone and M. Genovese, *Phys. Lett. B* **412**, 143 (1997).
- [66] A. Dainese (ALICE Collaboration), *Czech. J. Phys.* **55**, B367 (2005).
- [67] S. Cao, G.-Y. Qin, and S. A. Bass, *Phys. Rev. C* **92**, 024907 (2015).
- [68] J. W. Cronin, H. J. Frisch, M. J. Shochet, J. P. Boymond, P. A. Piroue, and R. L. Sumner, *Phys. Rev. D* **11**, 3105 (1975).
- [69] M. Lev and B. Petersson, *Z. Phys. C* **21**, 155 (1983).
- [70] A. Krzywicki, J. Engels, B. Petersson, and U. Sukhatme, *Phys. Lett. B* **85**, 407 (1979).
- [71] Z. Citron, A. Dainese, J. F. Grosse-Oetringhaus, J. M. Jowett, Y. J. Lee, U. A. Wiedemann, M. Winn, A. Andronic, F. Bellini, and E. Bruna, *CERN Yellow Rep. Monogr.* **7**, 1159 (2019).
- [72] G. Giacalone, J. Noronha-Hostler, M. Luzum, and J. Y. Ollitrault, *Phys. Rev. C* **97**, 034904 (2018).
- [73] C. Loizides, J. Kamin, and D. d'Enterria, *Phys. Rev. C* **97**, 054910 (2018).
- [74] K. J. Eskola, H. Niemi, R. Paatelainen, and K. Tuominen, *Phys. Rev. C* **97**, 034911 (2018).
- [75] S. Acharya *et al.* (ALICE Collaboration), *Phys. Lett. B* **790**, 35 (2019).